Mon. Not. R. Astron. Soc. **000**, 000–000 (0000) Printed 14 April 2016 (MN LATEX style file v2.2)

Quark deconfinement in the proto-magnetar model of Long Gamma-Ray Bursts

A. G. Pili[1,2⋆], N. Bucciantini[2,1], A. Drago[3], G. Pagliara[3], L. Del Zanna[1,2]
[1]*Dipartimento di Fisica e Astronomia, Università degli Studi di Firenze and INFN Sez. di Firenze, Via G. Sansone 1, I-50019 Sesto F. no (Firenze), Italy*
[2]*INAF - Osservatorio Astrofisico di Arcetri, Largo E. Fermi 5, I-50125 Firenze, Italy*
[3]*Dipartimento di Fisica e Scienze della Terra, Università di Ferrara and INFN Sez. di Ferrara, Via Saragat 1, I-44122 Ferrara, Italy*

Accepted / Received

ABSTRACT

We investigate the possible implications of quark deconfinement on the phenomenology of Long Gamma-Ray Bursts focusing, in particular, on the possibility to describe multiple prompt emission phases in the context of the *proto-magnetar model*. Starting from numerical models of rotating Hadron Stars and Quark Stars in full general relativity we track the electromagnetic spin-down evolution in both the hadronic and quark phase, linking the two families through conservation of baryon number and angular momentum. We give estimates of the timescales and the energetics involved in the spin-down process deriving, in the relevant spin range, the relation between the initial mass and the properties of deconfinement, whenever hadron-quark conversion is possible. We show how the results can be used with a relevant astrophysical cases such as the double burst GRB 110709B.

Key words: gamma-ray bursts - star: magnetar - star: neutron - dense matter - equation of state - gravitation

1 INTRODUCTION

The nature of the inner engine of Long Gamma-Ray Bursts (LGRBs) is still one of the most interesting and unsolved problems in astrophysics. While there is a compelling evidence that these events are associated with the core collapse of massive stars, it is not yet established whether the burst is produced by a disk accreting onto a black hole (within the so-called Collapsar model, Woosley 1993) or by the outflow emerging from a fast rotating and highly magnetized proto-neutron star (within the so-called proto-magnetar model, Metzger et al. 2011). It is also possible that both these systems contribute in producing LGRB events, depending on the initial conditions of the progenitor (in particular its mass, spin frequency and magnetic field). The SWIFT discovery of a late time activity, lasting up to 10^4 s and present in a sizable fraction of LGRBs, is more naturally interpreted within the proto-magnetar model as due to the pulsar-like energy injection powered by the residual rotational energy left after the prompt emission (Dall'Osso et al. 2011).

Within the proto-magnetar model, an important ingredient which regulates the temporal evolution of the jet and its gamma-ray luminosity is the neutrino signal released by the star due to deleptonization (the gradual neutronization of matter) and cooling. In particular, neutrinos ablate baryonic matter from the surface and provide a tiny amount of baryonic load which is crucial for an efficient internal dissipation of the kinetic energy of the jet into gamma emission. When the neutrino luminosity drops below $\sim 10^{50}$ erg/s (after a few tens of seconds), the magnetization (or the Lorentz factor) is too large and the prompt emission ends. It is not easy within the proto-magnetar model to reactivate the inner engine and therefore to describe multi-episodes of the prompt emission of LGRBs (Zhang et al. 2012) or X-ray flares occurring during the afterglow (Zhang et al. 2006).

The proto-magnetar model has been developed assuming that the newly born Compact Star (CS) is and remains a nucleonic star. Motivated by the measurements of very massive CSs (Demorest et al. 2010; Antoniadis et al. 2013) and the hints of the existence of very compact stellar objects (with radii close to 10km, Guillot et al. 2013; Özel et al. 2016), a two-families scenario has been recently proposed where both Hadronic Stars (HSs) and Quark Stars (QSs) exist in nature (Drago, Lavagno & Pagliara 2014; Drago et al. 2016; Drago & Pagliara 2016). Within this picture, a conversion of a HS into a QS can take place. In this paper we will discuss how this transition modifies the proto-magnetar model, revitalizing the inner engine. In particular, we will investigate the following scenario: i) a proto-magnetar is formed after a successful supernova explosion and its spinning down, which is responsible for the emission of a LGRB, leading to a gradual increase of the central density; ii) the increase of the density allows the formation of heavy hadrons such as Delta resonances and hyperons; iii) once a critical amount of strangeness is formed through hyperons at a density $\rho_{\rm crit}$, the HS converts (on a time-scale of the order of ten seconds) into a QS. This picture has been qualitatively discussed in Drago, Lavagno

⋆ E-mail: pili@arcetri.astro.it

& Pagliara (2014) for the case of non-rotating stars. Here we will improve that work by including rotation and spin-down evolution. Since both the initial hadronic and the final quark configurations are fast rotating stars, we compute the structure of rigidly rotating stars beyond the Hartle approximation (Hartle 1967) through the XNS code, which adopts the conformally-flat approximation for the space-time metric (see Bucciantini & Del Zanna 2011; Pili, Bucciantini & Del Zanna 2014, 2015; Bucciantini, Pili & Del Zanna 2015).

A distinctive feature of our two-families model is that the formation of a QS is accompanied by a rather large amount of energy released in the conversion, of the order of 10^{53} erg. Moreover, we will show that since the final QS configuration has a larger radius than the initial HS configuration, the conversion is accompanied by a significant increase of the momentum of inertia with a corresponding decrease of the rotational frequency. We will discuss possible phenomenological implications of the two-families scenario for the light curves of LGRBs in connection with late time activity emissions. For the case of quark stars there are two possible ways to produce a jet with the appropriate Lorentz factor. The first mechanism is based on the ablation of baryonic material from the surface of the star as long as the conversion front has not yet reached the surface (Drago & Pagliara 2016) A second mechanism is based on the rather large emission of electron-positron pairs from the surface of the bare quark star (Usov 1998, 2001; Page & Usov 2002). Both mechanism can be at work for producing late time activities.

In section 2 we describe our model and present our numerical result. In section 3 we conclude, discussing the phenomenological implications.

2 THE QUASI-STATIONARY EVOLUTION OF COMPACT STARS

In order to investigate the possible implications of the two-family of CSs scenario for the phenomenology of GRBs we have computed a large set of rigidly (rotation rate Ω = const) rotating equilibrium models for both HSs and QSs. Given the typical cooling properties of newly formed proto-neutron stars (Pons et al. 1999), the assumption of a cold star is justified at times larger than $\gtrsim$ 10 s after formation (the radius is relaxed to its final value). These numerical models are then linked together to describe the quasi-stationary evolution of CSs under the effect of the magnetic braking. With this simple approach we can give a preliminary estimate of both the timescales and the energetics involved in the spin-down before and after quark deconfinement, which we assume to happen when the central baryon density ρ_c reaches the critical values $\rho_{\rm crit} = 1.34 \times 10^{15}$ g/cm^3 (Drago, Lavagno & Pagliara 2014). We also derive the range of initial masses for which a delayed HS to QS conversion is possible.

Numerical models have been obtained using the equations of state discussed in Drago et al. (2016). The stars have been discretized with $\sim$ 500 grid points in both the radial and angular direction and Einstein equations are solved with a semi-spectral method using 20 spherical harmonics. Since the typical surface magnetic field invoked by the magnetar model for GRBs are of the order of 10^{15} G our models are computed neglecting magnetic field. Indeed, as discussed in Pili, Bucciantini & Del Zanna (2015), only central magnetic field strengths higher than $\sim 10^{16}$ G, corresponding to surface magnetic fields stronger than a few 10^{15} G, are able to modify the stellar global properties to a level appreciable with respect to the overall accuracy of the numerical scheme ($\lesssim 10^{-3}$). Hence

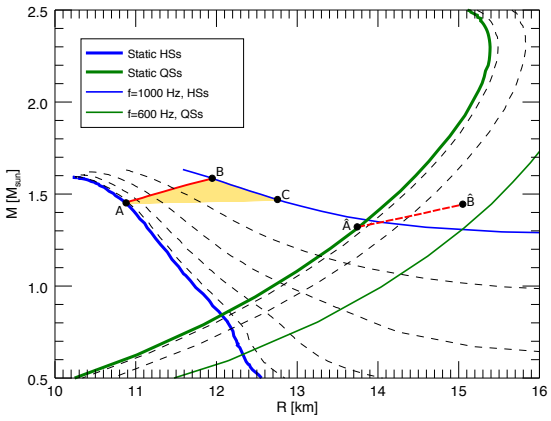

Figure 1. Gravitational mass as a function of the equatorial radius for both HSs and QSs. Thin dashed lines are sequences of constant frequency every 200 Hz from the non-rotating configurations (thick solid blue and green lines) to the configuration rotating at the maximum frequency (thin solid blue and green lines). The red solid line locates HSs with $\rho_c = \rho_{\rm crit}$. The yellow region shows the configurations centrifugally supported against deconfinement while the red dashed line locates QSs originating from the phase transition of HSs on top of the red solid line. Labeled configuration are discussed in the text.

we can safely assume that the stellar structure and the associated global quantities such as the gravitational mass M, the baryonic mass M_0 (a proxy for the total baryon number), the circumferential radius R and the Komar angular momentum J (for definitions see Pili, Bucciantini & Del Zanna 2014 and reference therein) do not depend on the magnetic field strength.

In the millisecond magnetar model for GRBs the typical rotation rates invoked in the literature (Metzger et al. 2011; Bucciantini et al. 2012) can be as high as $\sim$ 1 ms. The maximum rotation rate of compact stars at the end of deleptonization has been investigated in several papers (Goussard, Haensel & Zdunik 1998; Villain et al. 2004; Camelio et al. 2016). Its value depends on the initial physical conditions of the proto-neutron star (e.g. the entropy profile and a possible differential rotation) and on the compactness of the final cold and deleptonized configuration. If one adopts rather stiff equations of state, the maximum rotational frequency ranges between 300 and 600 Hz (Goussard, Haensel & Zdunik 1998; Villain et al. 2004; Camelio et al. 2016). In our analysis we use a rather soft hadronic equation of state (EoS) due to the formation of Delta resonances and hyperons and the maximum rotation frequency is expected to be larger. In the following we limit the computation of HS rotating models to a maximum frequency $f = 10^3$ Hz. On the other hand, for those QSs resulting from deconfinement it is sufficient to limit the spin frequency to 600 Hz. The results are shown in figure 1 where we plot the mass-radius relation for different sequences of CSs at constant spin frequency. There are two limiting configurations: the non-rotating configuration A with M(A) = $1.45 M_\odot$, M_0(A) = $1.67 M_\odot$ and R = 10.9 km; the 1 ms rotating configuration B with M(B) = $1.58 M_\odot$, M_0(B) = $1.82 M_\odot$ and R = 12 km. These define the mass range of interest for delayed quark deconfinement. The value of the critical mass of the configuration A cannot be determined with high precision not even in the scheme of the two families. The main uncertainties are due to the dynamics regulating the appearance of baryonic resonances and on the estimate of the

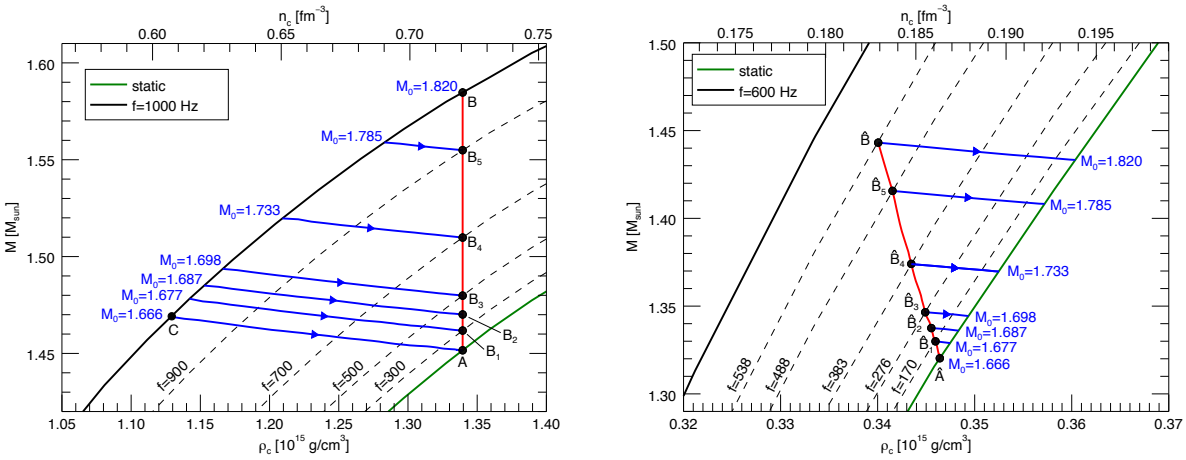

Figure 2. Gravitational mass against baryon central density for HSs (left panel) and QSs (right panel) sequences with constant spin frequency. In both cases the green solid lines represent the non-rotating sequences while the black solid lines are sequences rotating at the maximum spin frequency considered in this work: $1000Hz$ for HSs and $600Hz$ for QSs. Dashed lines are sequences with intermediate values of f while blue lines are equilibrium sequences at constant baryon mass M_0. Detailed results on configuration labeled with A and Bs are listed in table 1.

nucleation time of the first droplet of quark matter (Bombaci et al. 2016).

Massive HSs, that after their initial cooling (lasting for at most a few tens of seconds after core collapse) end above the red line in figure 1, have $\rho_c \geqslant \rho_{crit}$ and they will decay immediately to a QS. On the other hand those HSs having $M_0 < M_0(\mathrm{A})$ will never experience this transition[1]. Since for isolated CSs the baryonic mass is a conserved quantity, only those HSs having baryonic mass between $M_0(\mathrm{A})$ and $M_0(\mathrm{B})$ can migrate into the QS branch when their baryon central density rises to ρ_{crit} as a consequence of spin-down. The yellow shaded region of figure 1 shows these configurations. All the configurations having the same baryonic mass as A (for example the 1 ms rotator configuration C) take an infinite time to deconfine (deconfinement takes place at zero frequency). This same region is also shown in the left panel of figure 2 in terms of central baryon density ρ_c and gravitational mass M. Here blue lines are sequences of equilibria for given baryon mass and therefore they represent the evolutionary paths of HSs undergoing spin-down. Notice that along these sequences the variation of the gravitational mass, and hence of the total energy, is at most of the order of $\sim 1\%$.

As soon as the central density reaches the critical value the HS decays into a QS in $\lesssim 10$ s. Given the typical spindown timescales we assume that this transition is instantaneous and both the baryon number (baryonic mass) and the angular momentum J are conserved. The red dashed line in figure 1 and in the right panel of figure 2 maps upon the QS sequences the configurations which originate from quark deconfinement of HSs. With reference to our limiting configurations, the HS labeled with A migrates to the configuration $\hat{\mathrm{A}}$ with gravitational mass $M(\hat{\mathrm{A}}) = 1.32M_\odot$, while the HS B migrates to the configuration $\hat{\mathrm{B}}$ with $M(\hat{\mathrm{B}}) = 1.44M_\odot$. In both cases the total energy released in the transition is of the order of $\sim 0.1M_\odot$. Finally, after the formation, QSs can spin-down following the evolutionary path of constant M_0 showed in the right panel of figure 2.

[1] For simplicity, we are not considering here the process of nucleation of quark matter (Bombaci et al. 2016). In a more realistic case the red lines connecting the configurations A and B would transform in a strip whose width is connected to the nucleation time.

Table 1. Global quantities at the phase transition for the configurations labeled in figure 2: gravitational mass M and spin frequency f of the hadronic configuration at deconfinement; difference between the spin frequency Δf_d, the gravitational mass ΔM_d, and the rotational energy ΔK_d before and after deconfinement.

Label	M_0 $[M_\odot]$	f [Hz]	Δf_d [Hz]	M $[M_\odot]$	ΔM_d $[M_\odot]$	ΔK_d $[10^{52}$ erg]
A	1.666	0.00	0.00	1.452	0.132	0.00
B_1	1.677	300	130	1.462	0.132	0.20
B_2	1.687	400	177	1.470	0.133	0.35
B_3	1.698	500	224	1.480	0.133	0.57
B_4	1.733	700	317	1.520	0.136	1.18
B_5	1.785	900	413	1.555	0.139	2.14
B	1.820	1000	462	1.585	0.142	2.80

Detailed results are presented in table 1 where we list the variation of the spin frequency Δf_d, of the gravitational mass ΔM_d and of the rotational kinetic energy ΔK_d (where $K := \frac{1}{2} J\Omega$) during the phase transition for a set of selected models. Since QSs have larger radii and hence also a larger moment of inertia, conservation of the angular momentum implies a drop in spin frequency. Interestingly we found that the variation of the stellar radius is slightly larger ($\sim 10\%$ between cases A and B) at higher M_0. Hence transitions at higher M_0 are characterized by a bigger percent variation of the spin frequency and of the rotational energy. ΔK_d only accounts for the variation of the kinetic energy while the total change of energy is given by the variation of the gravitational mass ΔM_d and it will produce a reheating of the star. In the range of interest, $\Delta M_d \simeq 10^{53}$ erg and $\Delta K_d \simeq 10^{51-52}$ erg. This significant amount of energy released by quark deconfinement can be associated with a late time activity as we will discuss in the following.

In the magnetar GRB model the spindown evolution is governed by magnetic torques. Therefore in order to evaluate the evolutionary timescales of our models we solve, for simplicity, the spindown formula for an aligned dipole rotator (Spitkovsky 2006):

$$\frac{\mathrm{d}J}{\mathrm{d}t} = -\frac{B^2 R^6 \Omega^3}{4}, \qquad (1)$$

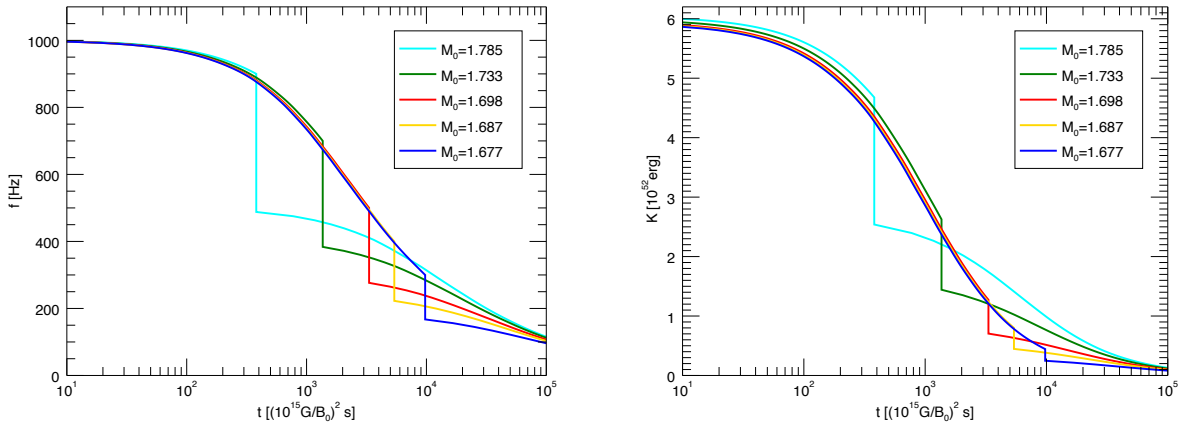

Figure 3. Time evolution of the spin-frequency (left panel) and of the rotational energy (right panel) for dipole magnetic field losses along sequences of constant baryonic mass M_0.

Table 2. Spin-down timescales to quark deconfinement $\Delta t_{\rm sd}$ together with the associated variation of the rotational kinetic energy $\Delta K_{\rm sd}$ starting from an initial spin period P_i for the equilibrium sequences shown in figure 3. We also report the spin-down timescales $\Delta t_{\rm q}$ (defined as the time needed to half the rotational frequency of the QS) and the corresponding rotational energy loss $\Delta K_{\rm q}$ after quark deconfinement. The initial magnetic field is of 10^{15} G.

M_0 $[M_\odot]$	$P_i \rightarrow P_{\rm d}$ [ms]	$\Delta t_{\rm sd}$	$\Delta K_{\rm sd}$ $[10^{52}$ erg]	$\Delta t_{\rm q}$	$\Delta K_{\rm q}$ $[10^{52}$erg]
1.666	$1.0 \rightarrow \infty$	∞	5.91	-	-
1.677	$1.0 \rightarrow 3.3$	2.7 hr	5.48	37 hr	0.19
	$2.0 \rightarrow 3.3$	1.8 hr	0.82		
	$3.0 \rightarrow 3.3$	37 min	0.13		
1.687	$1.0 \rightarrow 2.5$	1.5 hr	5.13	21 hr	0.33
	$2.0 \rightarrow 2.5$	36 min	0.46		
1.698	$1.0 \rightarrow 2.0$	55 min	4.68	14 hr	0.53
1.733	$1.0 \rightarrow 1.4$	23 min	3.37	8.2 hr	1.20
1.785	$1.0 \rightarrow 1.1$	6 min	1.37	5.4 hr	1.95
1.820	$1.0 \rightarrow 1.0$	0	0	4.6 hr	2.41

where B is the magnetic field strength at the pole and we assume that the magnetic flux $\Phi = BR^2$ is constant during the evolution. This choice gives only an upper limit to the timescale for deconfinement: oblique rotators or mass loaded winds can have higher torques (Metzger et al. 2011) that can lead to faster spin-down (up to a factor 10) in the first tens of seconds. Furthermore we neglect the possibility of late time mass accretion (Bernardini et al. 2014), because it introduces extra degree of freedom that cannot be easily constrained. Moreover we also neglect gravitational waves emission which is relevant only if the star owns a very strong internal toroidal field larger than $\sim 10^{16}$ G (Dall'Osso, Shore & Stella 2009). In the mass range of interest we have evaluated the spin-down timescale up to deconfinement, which is shown in figure 3 and table 2, for each equilibrium sequence of constant M_0 , assuming an initial surface magnetic field $B_0 = 10^{15}$ G. Note that the spindown age scales with B_0^{-2}. Conservation of the magnetic flux Φ is also assumed to hold during the phase transition. The resulting magnetic field strength is of the order of $0.5B_0$ due to the change of the stellar radius.

The time evolution of the spin frequency f and of the rotational energy K is shown in figure 3 for the HS configurations labelled $B_1 - B_5$. It is evident that HSs with higher mass have a shorter lifetime before deconfinement, since they reach the critical density at higher spin frequencies. In table 2 we list the time it takes to deconfinement and the associated rotational spin down energy loss $\Delta K_{\rm sd}$ for different values for the initial spin-period.

3 DISCUSSION AND CONCLUSIONS

Let us consider now the phenomenological implications of our scenario for the evolution of proto-magnetars. The variation of the rotational energy $\Delta K_{\rm sd}$ displayed in table 2 gives an estimate of the energy reservoir available to the HS before deconfinement which occurs after a spin-down time scale $\Delta t_{\rm sd}$ that ranges from several minutes to hours. Comparing $\Delta K_{\rm sd}$ with the typical energetics of the millisecond magnetar model for GRBs (figure 19 of Metzger et al. 2011) one notices that the values shown in table 2 are compatible with the requirement for classical GRBs, being $\Delta K_{\rm sd}$ much larger than 10^{50-51} erg, i.e. the typical energy emitted in X-rays and in γ-ray during GRB events. We also remark that since $\Delta t_{\rm sd}$ is much larger than the typical duration of the prompt phase of LGRBs, deconfinement does not spoil the nice description of the prompt emission of LGRBs within the proto-magnetar model.

However, as discussed before, also the HS to QS transition is characterized by a huge release of energy (table 1) that in principle could manifest itself as a second transient. Hence the time for deconfinement $\Delta t_{\rm d}$ is indicative of the delay between the prompt GRB emission due to the HS and the possible flare or second prompt emission associated to quark deconfinement. Let us summarize how the deconfinement process proceeds and how is the energy released. As studied in Drago & Pagliara (2015), deconfinement can be described as a combustion process which can be separated in two phases. The first phase is very rapid due to turbulence and it converts the bulk of the star in a time scale of few ms (Drago, Lavagno & Parenti 2007; Herzog & Ropke 2011). The second phase is dominated by diffusion of strangeness and it is therefore much slower, typically lasting a few tens of seconds (Drago & Pagliara 2015) The huge energy associated to deconfinement is released via thermal neutrinos whose luminosity can similarly be divided into an initial peak associated with the deconfinement of the bulk of the star and a lower quasi-plateaux emission associated with

the burning of the external layer of the star. The interaction of neutrinos with the material of the crust of the star causes the ablation of baryons which plays a crucial role in the proto-magnetar model of GRBs. A distinctive feature of the formation of a quark star is the rapid suppression of the baryonic flux once the conversion front reaches the surface of the star. This poses an upper limit to the duration of an event of the prompt emission if described within the proto-magnetar model and associated with the baryonic emission from the surface of a star undergoing quark deconfinement. However, also the lepton emission from surface of the bare quark star (Usov 1998, 2001; Page & Usov 2002) can be used to produce a jet.

As an example we discuss the case of GRB 110709B characterized by two sub-bursts of observed duration respectively $\Delta t^{(1)} \sim 80$ s and $\Delta t^{(2)} \sim 300$ s, separated by a delay $\Delta t_{\rm delay} \sim 600$ s (Zhang et al. 2012; Penacchioni et al. 2013). Neither the cosmological redshift nor the energetics of the event are well determined and in the following we adopt values compatible with the analysis by Penacchioni et al. (2013), being in agreement with the pulse-wise Amati relation (Basak & Rao 2013). In particular we assume an isotropic energy $E^{(1)}_{\rm iso} = 2.6 \times 10^{53}$ erg for the first burst and $E^{(2)}_{\rm iso} = 4.4 \times 10^{52}$ erg for the second one at redshift $z = 1$. We further assume a beaming correction of $\sim 10^{-2}$ in line with average jet opening angle of LGRB (Guidorzi et al. 2014). Requiring that during the bursting events (radiatively-efficient phases) the mass loading enhances the spin-down by a factor $3 - 4$ with respect to the force-free case (Metzger et al. 2011), we find that, assuming an initial magnetic field $B = 2 \times 10^{15}$ G, HSs with initial spin period in the range $1 - 1.6$ ms and baryon masses in $M_0 = 1.72 - 1.70 M_\odot$ have enough rotational energy to power the first event in a time $\Delta t^{(1)}$, deconfine with a delay $\Delta t_{\rm delay}$ and originate a QS rotating fast enough to power also the second event on the required time $\Delta t^{(2)}$. Notice that the requirements of short delays and fast rotating QS select for configurations with high baryon mass. On the contrary HSs with lower M_0 take longer to decay and form a slowly rotating QS that at most could power weak flaring events in the afterglows, on timescale of few hours (see table 2).

Finally, let us clarify how deconfinement can be responsible of rather long gamma emissions, as in the case of GRB 110709B, and also of the prompt phase of short GRBs, as discussed in Drago & Pagliara (2016); Drago et al. (2015). The main differences are related to the neutrinos' flux and energy which determine the baryonic mass ejection rate. In the case of sGRBs, the neutrino flux is significantly larger (of at least one order of magnitude) mainly because of the larger mass of the forming QS. Also the neutrino energy is larger roughly by a factor of three. This implies that the phase during which the QS forms cannot produce a large enough Lorentz factor in the case of sGRBs. At variance, in the case of LGRBs, the mass ejection rate is not too large and the prompt emission can start almost immediately at the beginning of deconfinement.

Although our model requires further investigation for a detailed assessment, our simple analysis of the spin-down evolution of CSs provides us with a new characterization, in terms of energetics and timescales, of the possible observational signatures associated with the two-families scenario. In particular we have shown, with reference to double GRBs, how, once the EoSs of HSs and QSs are chosen, the associated phenomenology is constrained by the initial magnetic field strength, initial rotational period and the stellar mass. This implies that, in principle, new observations, could validate the two-families hypotheses, gaining new insights in the physic of dense matter.

ACKNOWLEDGEMENTS

This work has been supported by an EU FP7-CIG grant issued to the NSMAG project (PI: NB), and by the INFN TEONGRAV initiative (local PI: LDZ).

REFERENCES

Antoniadis J. et al., 2013, Science, 340, 448
Basak R., Rao A. R., 2013, MNRAS, 436, 3082
Bernardini M. G. et al., 2014, MNRAS, 439, L80
Bombaci I., Logoteta D., Vidaña I., Providência C., 2016, European Physical Journal A, 52, 58
Bucciantini N., Del Zanna L., 2011, A&A, 528, A101
Bucciantini N., Metzger B. D., Thompson T. A., Quataert E., 2012, MNRAS, 419, 1537
Bucciantini N., Pili A. G., Del Zanna L., 2015, MNRAS, 447, 3278
Camelio G., Gualtieri L., Pons J. A., Ferrari V., 2016, ArXiv e-prints
Dall'Osso S., Shore S. N., Stella L., 2009, MNRAS, 398, 1869
Dall'Osso S., Stratta G., Guetta D., Covino S., De Cesare G., Stella L., 2011, Astron. Astrophys., 526, A121
Demorest P., Pennucci T., Ransom S., Roberts M., Hessels J., 2010, Nature, 467, 1081
Drago A., Lavagno A., Metzger B., Pagliara G., 2015, ArXiv e-prints
Drago A., Lavagno A., Pagliara G., 2014, Phys. Rev. D, 89, 043014
Drago A., Lavagno A., Pagliara G., Pigato D., 2016, European Physical Journal A, 52, 40
Drago A., Lavagno A., Parenti I., 2007, Astrophys. J., 659, 1519
Drago A., Pagliara G., 2015, Phys. Rev. C, 92, 045801
—, 2016, European Physical Journal A, 52, 41
Goussard J.-O., Haensel P., Zdunik J. L., 1998, A&A, 330, 1005
Guidorzi C. et al., 2014, MNRAS, 438, 752
Guillot S., Servillat M., Webb N. A., Rutledge R. E., 2013, Astrophys. J., 772, 7
Hartle J. B., 1967, ApJ, 150, 1005
Herzog M., Ropke F. K., 2011, Phys. Rev., D84, 083002
Metzger B. D., Giannios D., Thompson T. A., Bucciantini N., Quataert E., 2011, MNRAS, 413, 2031
Özel F., Psaltis D., Güver T., Baym G., Heinke C., Guillot S., 2016, ApJ, 820, 28
Page D., Usov V. V., 2002, Phys. Rev. Lett., 89, 131101
Penacchioni A. V., Ruffini R., Bianco C. L., Izzo L., Muccino M., Pisani G. B., Rueda J. A., 2013, A&A, 551, A133
Pili A. G., Bucciantini N., Del Zanna L., 2014, MNRAS, 439, 3541
—, 2015, MNRAS, 447, 2821
Pons J. A., Reddy S., Prakash M., Lattimer J. M., Miralles J. A., 1999, ApJ, 513, 780
Spitkovsky A., 2006, ApJLett, 648, L51
Usov V. V., 1998, Phys. Rev. Lett., 80, 230
Usov V. V., 2001, ApJLett, 550, L179
Villain L., Pons J. A., Cerdá-Durán P., Gourgoulhon E., 2004, A&A, 418, 283
Woosley S. E., 1993, ApJ, 405, 273
Zhang B., Fan Y. Z., Dyks J., Kobayashi S., Mészáros P., Burrows D. N., Nousek J. A., Gehrels N., 2006, ApJ, 642, 354
Zhang B.-B. et al., 2012, ApJ, 748, 132